

Quantum engineering of a low-entropy gas of heteronuclear bosonic molecules in an optical lattice

Lukas Reichsöllner^{1,*}, Andreas Schindewolf^{1,*}, Tetsu Takekoshi^{1,2}, Rudolf Grimm^{1,2}, and Hanns-Christoph Nägerl¹

¹*Institut für Experimentalphysik, Universität Innsbruck, 6020 Innsbruck, Austria*

²*Institut für Quantenoptik und Quanteninformation, Österreichische Akademie der Wissenschaften, 6020 Innsbruck, Austria*

(Dated: March 13, 2022)

We produce low-entropy samples of ultracold $^{87}\text{Rb}^{133}\text{Cs}$ Feshbach molecules in an optical lattice with a filling fraction exceeding 30%. Starting from two spatially separated Bose-Einstein condensates of Rb and Cs atoms, Rb-Cs atom pairs are efficiently produced in a sample mixing process that utilizes the superfluid-to-Mott insulator quantum phase transition twice, first for the Cs sample, then for the Rb sample, after nulling the Rb-Cs interaction at a Feshbach resonance's zero crossing. We characterize the mixing process in terms of sample overlap and mixing speed. The dense and ultracold sample of more than 5000 RbCs molecules is an ideal starting point for experiments in the context of quantum many-body physics with long-range dipolar interactions.

PACS numbers: 05.30.Rt, 37.10.Jk, 67.85.-d

Samples of dipolar ground-state molecules with low entropy offer a platform for exploring new areas of quantum many-body physics and related fields. Due to their long-range, spatially anisotropic interaction they have been proposed to enable investigations into novel forms of quantum matter, e.g. supersolidity, unconventional manifestations of superfluidity, and novel types of quantum magnetism [1–3]. They are expected to allow the realization of many-body spin systems [4] with, in principle, local spin control and readout. In particular, they promise the study of dynamical processes in such systems, e.g. on many-body spin transport and inhibition thereof [5]. In addition, with the exquisite control over all quantum degrees of freedom, they offer the possibility of implementing quantum simulation protocols [6] that require genuine and strong long-range interactions.

The production of low-entropy samples of rovibronic ground-state molecules is challenging. To date, the regime of nanokelvin molecular temperatures has only been reached for a selected class of dimer molecules by combining the technique of Feshbach association in ultracold, nearly quantum degenerate, atomic samples with the technique of stimulated ground-state transfer (stimulated Raman adiabatic passage, STIRAP) as pioneered on homonuclear Rb_2 and Cs_2 [7–9] and heteronuclear fermionic KRb [10]. This strategy has recently been applied to various other heteronuclear alkali combinations, i.e. to bosonic RbCs [11, 12], fermionic NaK [13], and bosonic NaRb [14]. In essence, low entropy is obtained on the atomic samples, and Feshbach association and subsequent STIRAP transfer are aimed at maintaining low entropy.

For the efficient creation of heteronuclear molecules

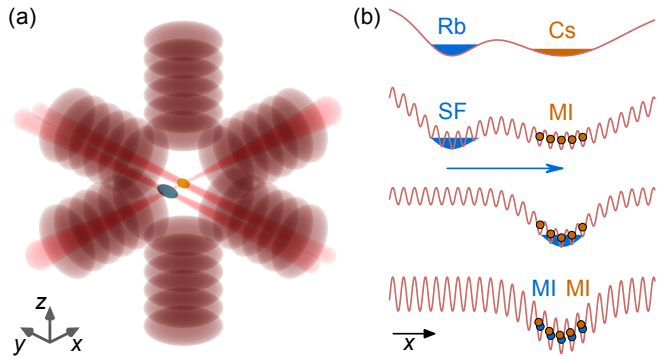


FIG. 1: (Color online). Simplified experimental optical trap setup and overlap strategy. (a) Bose-Einstein condensates of Rb (blue) and Cs (orange) are initially produced in separate crossed dipole traps. They are merged along the direction of one of the trapping beams (x -direction) at the center of a six-beam optical lattice (standing waves as indicated, center part omitted for clarity). (b) Starting from the two BEC's, the lattice first induces a one-atom Mott insulator (MI) for the Cs sample. The Rb sample, yet superfluid (SF), is brought into overlap with the Cs sample by precisely moving the underlying dipole trap beam. The lattice is raised further to create a double-species MI with high Rb-Cs atom pair fraction.

the mixing of the atomic samples is of crucial importance. Maintaining low entropy in the course of the mixing process and during the subsequent association step poses a great experimental challenge. Ideally, each atom from one species should find precisely one atom from the other species for pairing up. Loss processes due to atomic three-body recombination (before the association process) and vibrational relaxation as a result of either atom-molecule or molecule-molecule collisions (after the association process) should be avoided. It is difficult to prevent these loss processes, and all experiments with 3D bulk mixtures [10–14] have been able to convert only a comparatively small fraction of the initial heteronuclear

*These authors contributed equally to this work.

atomic mixture to molecules, which has led to a significant increase of the systems' entropy.

In this Letter, we demonstrate a general sample-mixing technique that allows us to efficiently produce heteronuclear atom pairs at the individual lattice sites of an optical lattice and thereby to prepare low-entropy samples of heteronuclear dimer molecules. With this technique we can mix nominally immiscible bosonic atom samples while largely avoiding three-body losses. Our quantum engineering approach combines superfluid transport with interspecies interaction control and atom localization as a result of the superfluid (SF) to Mott-insulator (MI) quantum phase transition. Specifically, in a non-trivial generalization of the work with homonuclear molecules [9], we prepare heteronuclear Rb-Cs atom pairs at high lattice filling by employing the SF to MI transition twice, first for the Cs sample to create a one-atom-per-site Cs MI, then for the Rb sample on top of the Cs MI with the aim to create a flat distribution of Rb-Cs atom pairs [9]. These pairs are subsequently converted to RbCs molecules. Control of the interspecies interaction at an interspecies Feshbach resonance's zero crossing is needed to allow for sample mixing. Our technique minimizes loss since the lattice greatly suppresses atomic three-body processes and shields the Rb-Cs atom pairs and the subsequently formed RbCs molecules from collisions. Recently, with some similarity to our work, low-entropy samples of fermionic KRb ground-state molecules [15, 16] have been produced in a optical lattice by forming atom pairs from a band insulator for K on top of a MI for Rb.

The experiment starts with spatially separated Bose-Einstein condensates (BEC) of ^{133}Cs and ^{87}Rb atoms, levitated against gravity and trapped in crossed dipole traps as shown schematically in Fig. 1(a) and (b) [17, 18]. The initial distance between the samples in the horizontal plane is $x = 100 \mu\text{m}$. Typically, we have 4.0×10^4 atoms in the Rb BEC and 1.7×10^4 atoms in the Cs BEC at a magnetic offset field $B \approx 21.0 \text{ G}$. At this field value, which is suitable for producing the Cs BEC [19], the Rb-Rb and the Cs-Cs intraspecies scattering lengths are $a_{\text{RbRb}} \approx 100 a_0$ and $a_{\text{CsCs}} \approx 220 a_0$, respectively, while the interspecies scattering length is $a_{\text{RbCs}} \approx 645 a_0$ [20], rendering the two BEC's immiscible. Here, Cs (Rb) is in the $f_{\text{Cs}} = 3, m_{f_{\text{Cs}}} = 3$ ($f_{\text{Rb}} = 1, m_{f_{\text{Rb}}} = 1$) spin state. A 3D cubic optical lattice, generated by three retro-reflected laser beams at $\lambda = 1064.5 \text{ nm}$ with large $1/e^2$ -waists of about $450 \mu\text{m}$ covering both samples, is ramped up to induce the SF-to-MI phase transition for the Cs sample. At a lattice depth of $V_{\text{mix}}^{\text{Cs}} = 20 E_{\text{rec}}^{\text{Cs}}$, where $E_{\text{rec}}^{\text{Cs}} = h^2/(2m_{\text{Cs}}\lambda^2)$ is the Cs photon recoil energy, we create a one-atom-per-site MI for Cs [17]. Typically, 80% of the atoms in the initial Cs BEC are found to be in the one-atom-Mott shell [21]. The Rb sample, which sees a depth of $V_{\text{mix}}^{\text{Rb}} \approx 7.7 E_{\text{rec}}^{\text{Rb}}$, is still superfluid. Here, $E_{\text{rec}}^{\text{Rb}} = h^2/(2m_{\text{Rb}}\lambda^2)$ is the Rb photon recoil energy. The Rb sample, over the course of the next 1500 ms, is steered

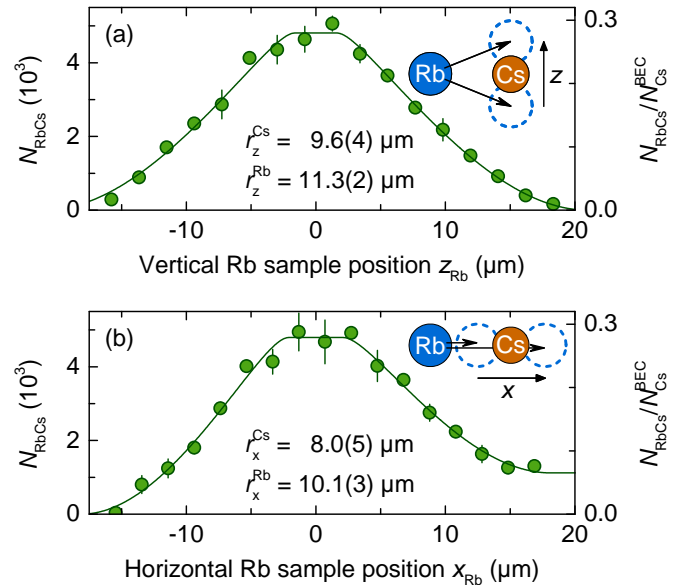


FIG. 2: (Color online). Sample spatial overlap. Number of Feshbach molecules N_{RbCs} and normalized number $N_{\text{RbCs}}/N_{\text{Cs}}^{\text{BEC}}$ as a function of (a) Rb sample vertical position z_{Rb} and (b) Rb sample horizontal position x_{Rb} as indicated by the cartoons. Each data point is the average of 3 experimental runs, and the error bars indicate the standard error. The solid lines in (a) and (b) are simple fits to the data to extract the sample radii $r_z^{\text{Cs}}, r_z^{\text{Rb}}, r_x^{\text{Cs}},$ and r_x^{Rb} as indicated, assuming the convolution of spherical samples with homogenous densities and taking into account the trailing tail by allowing for a one-sided offset [17].

onto the Cs sample by moving the underlying dipole trap beam linearly in time [17]. Before the two samples start to overlap, the field B is increased to $B \approx 354.95 \text{ G}$ to access an interspecies Feshbach resonance's zero crossing with slope $da_{\text{RbCs}}/dB = 0.30 a_0/\text{mG}$ [17]. Note that in the vicinity of the interspecies Feshbach resonance a_{CsCs} is prohibitively large, $a_{\text{CsCs}} \approx 2500 a_0$ [22]. A mixed sample without the lattice would experience rapid Cs-Cs-Cs and Cs-Cs-Rb three-body loss. The lattice thus assures sufficient stability over the course of the mixing process.

After spatial overlap, the lattice depth is further raised to $V_{\text{fin}}^{\text{Cs}} = 36 E_{\text{rec}}^{\text{Cs}}$ ($V_{\text{fin}}^{\text{Rb}} = 13.8 E_{\text{rec}}^{\text{Rb}}$) by a linear ramp over the course of 40 ms. This now induces the SF-to-MI transition on the Rb sample on top of the Cs sample, localizing Rb atoms and hence producing Rb-Cs atom pairs at the individual sites of the lattice. We note that we reach the phase transition point but do not enter deeply into the MI regime for Rb because of limited laser power. To quantify the success of mixing process, we associate the Rb-Cs atom pairs to RbCs Feshbach molecules by ramping down B across the resonance pole at 352.74 G. Further lowering B to below 315 G allows us to enter a Feshbach state with a much lower magnetic moment than the initial molecular state [17]. The number of molecules N_{RbCs} is determined via Stern-Gerlach sep-

ration of atoms and molecules followed by reversing the association path to dissociate the molecules and measuring the number of atoms that have previously been bound in a molecule [11, 20]. Note that the molecular sample is essentially frozen in the lattice since the molecular mobility is much lower than the atomic mobility as a result of higher mass and higher polarizability. Each molecule resides in the lowest vibrational quantum state of its respective lattice well [9], as can be checked in a band-mapping experiment. Our figure of merit is $N_{\text{RbCs}}/N_{\text{Cs}}^{\text{BEC}}$, where $N_{\text{Cs}}^{\text{BEC}}$ is the (constant) number of Cs atoms in the initial BEC, giving us a lower bound for the lattice filling fraction p [17]. We note that, up to this point, we have lost about 50% of the atoms that were in the initial Cs BEC: About 15% of the Cs atoms are lost irrespective of the Rb sample. Additional 35% are lost when the two samples are allowed to interact, presumably due to interspecies three-body recombination. Further details on experiment timing, Feshbach structure, and sample characterization are given in Ref. [17].

First we address the samples' spatial overlap. We vary the final position of the Rb sample in horizontal x - and vertical z -direction and plot N_{RbCs} respectively $N_{\text{RbCs}}/N_{\text{Cs}}^{\text{BEC}}$ as a function of the final position as shown in Fig. 2(a) and (b). For this set of data, we form up to 5000 RbCs molecules when the spatial overlap is maximal. When varying z , we record data that is optimized as a function of x , and vice-versa. The data clearly shows the spatial convolution of the two samples. It allows us to estimate the sample extent as indicated in Fig. 2(a) and (b) [17]. Also, it shows that we control the relative positions of the two samples to much better than their sizes. When varying the vertical position, the data is symmetric around the origin as one may expect. However, varying the horizontal position shows a clear asymmetry. We attribute this asymmetry to a trailing tail that the Rb sample develops during transport. The origin of the tail and whether its existence limits our pair formation efficiency will have to be addressed in future work.

Next, we characterize the mixing process in terms of the interspecies interaction strength. Fig. 3(a) shows the result of our measurements for optimal spatial overlap when we choose different values for a_{RbCs} in the vicinity of the zero crossing during the mixing process. The efficiency is maximal for nulled interactions and it drops off for repulsive and attractive interactions with an initial slope of $\sim \pm 0.1/50 a_0^{-1}$. At maximum, our figure-of-merit $N_{\text{RbCs}}/N_{\text{Cs}}^{\text{BEC}}$ is significantly above 30%. Interestingly, the data is not symmetrically distributed about the origin. There is a steep edge at $a_{\text{RbCs}} \approx -80 a_0$. The reason for this edge is not entirely clear, but it coincides with the resonance condition $U_{\text{RbCs}} = -U_{\text{RbRb}}$, where U_{RbCs} (U_{RbRb}) is the Hubbard onsite interaction energy [17] for Rb-Cs (Rb-Rb) atom pairs. When this condition is fulfilled, a Rb atom can resonantly tunnel onto a

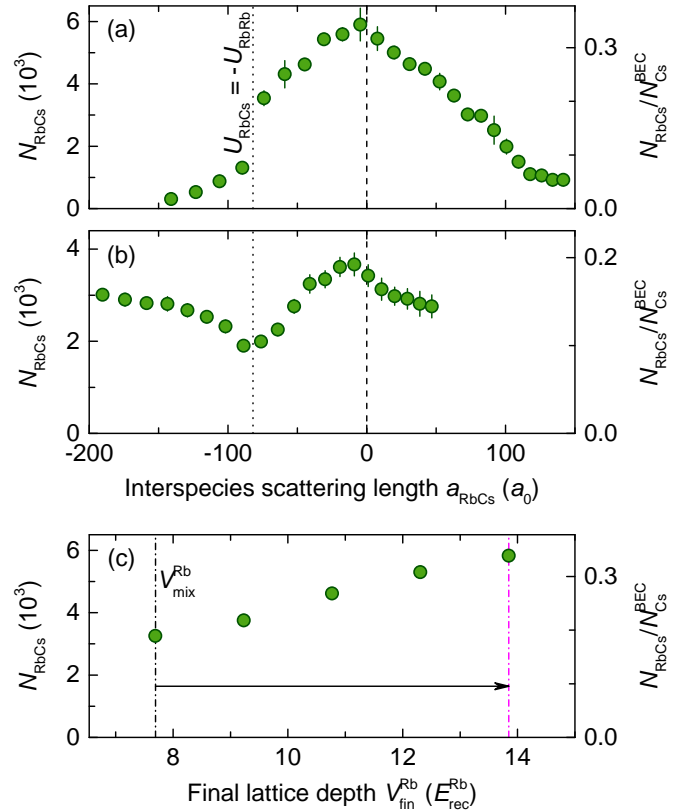


FIG. 3: (Color online). (a) Characterization of mixing process. Number of Feshbach molecules N_{RbCs} respectively normalized number $N_{\text{RbCs}}/N_{\text{Cs}}^{\text{BEC}}$ as a function of the interspecies scattering length a_{RbCs} . The vertical dotted line at $a_{\text{RbCs}} = -82 a_0$ indicates the resonance condition $U_{\text{RbCs}} = -U_{\text{RbRb}}$ as discussed in the text. (b) Loss of Rb-Cs atom pairs due to Rb tunneling as quantified by N_{RbCs} respectively $N_{\text{RbCs}}/N_{\text{Cs}}^{\text{BEC}}$ after a fixed hold time $\tau = 270$ ms upon ramping a_{RbCs} within 10 ms to the value as indicated. (c) Mixing efficiency as quantified by N_{RbCs} respectively $N_{\text{RbCs}}/N_{\text{Cs}}^{\text{BEC}}$ as a function of final lattice depth $V_{\text{fin}}^{\text{Rb}}$ as seen by the Rb atoms. The data shown in (a), (b), and (c) is the average of 3, 6 to 11, and 6 runs of the experiment, respectively, and the error bars reflect the standard error.

site occupied by a Rb-Cs atom pair. This should lead to enhanced Rb-Rb-Cs three-body loss in the course of the overlap procedure. To test this hypothesis, we have performed an experiment in which we first prepare Rb-Cs atom pairs as discussed before at optimal efficiency, but without the subsequent step of Feshbach association. Instead, we hold the atom pairs for $\tau = 270$ ms at various values for a_{RbCs} . During this time, Rb atoms, although with low mobility, are able to tunnel. We then stop the evolution and determine the number of Rb-Cs atom pairs as before via Feshbach association, Stern-Gerlach separation, and molecule detection. Fig. 3(b) shows the result. A clear minimum can be found for N_{RbCs} that coincides with the resonance condition. Note that the data shows a maximum that is slightly shifted away from $a_{\text{RbCs}} = 0$

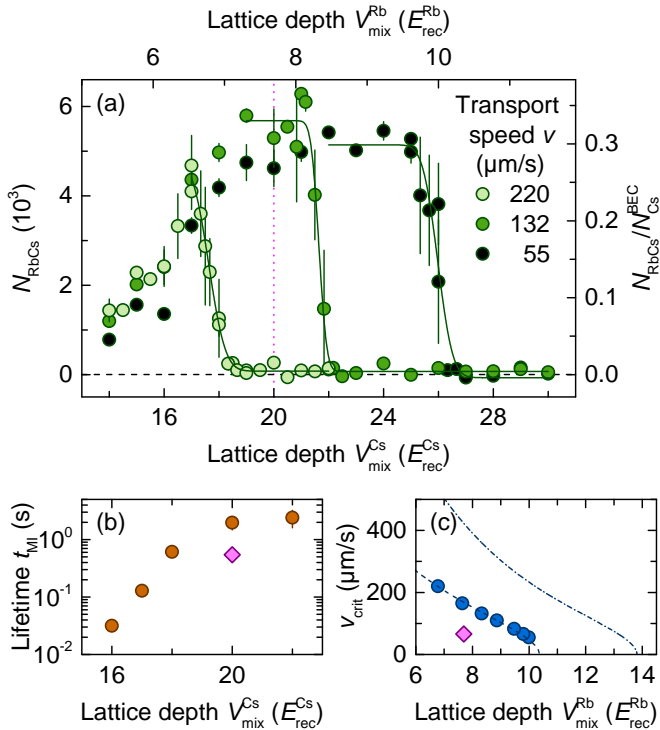


FIG. 4: (Color online). Mixing speed limit. (a) Mixing efficiency as quantified by N_{RbCs} respectively $N_{\text{RbCs}}/N_{\text{Cs}}^{\text{BEC}}$ as a function of lattice depth $V_{\text{mix}}^{\text{Rb}}$ respectively $V_{\text{mix}}^{\text{Cs}}$ during mixing for various transport speeds as indicated. The solid lines are error-function fits to determine the critical lattice depth. (b) Lifetime t_{MI} of the Cs one-atom Mott insulator (circles) as a function of lattice depth V_{lat} at $a_{\text{CsCs}} \approx 2500 a_0$. The diamond indicates the duration of the mixing process at the mixing lattice depth $V_{\text{mix}}^{\text{Cs}} = 20 E_{\text{rec}}^{\text{Cs}}$. (c) Critical transport speed v_{crit} (circles) as determined from data shown in (a) as a function of lattice depth $V_{\text{mix}}^{\text{Rb}}$ during mixing. The diamond indicates the conditions used in most experiments reported here. The dashed-dotted line is the theory prediction from Ref. [23]. The dashed line through the data is the same prediction but shifted horizontally by $3.5 E_{\text{rec}}^{\text{Rb}}$. The error bars reflect the standard error.

towards negative values. We have no immediate explanation for this.

In the next experiment we test how the molecule production efficiency depends on the final lattice depth $V_{\text{fin}}^{\text{Rb}}$. For this, we raise the lattice to a value in the range between $7.7 E_{\text{rec}}^{\text{Rb}}$ (no raise) and $13.8 E_{\text{rec}}^{\text{Rb}}$ (at full laser power available) with a linear ramp as before and we again determine N_{RbCs} . Note that the Rb sample is expected to undergo the SF-to-MI phase transition at $V_{\text{crit}}^{\text{Rb}} \approx 13.8 E_{\text{rec}}^{\text{Rb}}$. The data for N_{RbCs} , shown in Fig. 3(c), shows no indication of saturation. We thus may expect that the efficiency can be improved by driving the Rb sample more deeply into the MI phase.

Finally, we address the question how quickly the two samples can be merged. Evidently, a fast merger is desirable in order to reduce the effect of loss processes as a

result of three-body recombination or heating processes due to laser-intensity noise and beam-pointing instabilities. We vary the speed v at which we steer the Rb dipole trap towards and onto the Cs sample and then determine N_{RbCs} as before. The data, as a function of mixing lattice depth $V_{\text{mix}}^{\text{Rb}}$ respectively $V_{\text{mix}}^{\text{Cs}}$ is shown in Fig. 4(a). For a given v , as $V_{\text{mix}}^{\text{Rb}}$ is increased, the mixing process first becomes more efficient, but then experiences an abrupt breakdown at specific values $V_{\text{crit}}^{\text{Rb}}$ that we determine by error-function fits to the data [17]. For sufficiently low speeds (see e.g. the data for $v = 55 \mu\text{m/s}$) the efficiency saturates before it experiences the breakdown. We can explain the reduction of efficiency towards lower $V_{\text{mix}}^{\text{Rb}}$ by a reduced lifetime of the Cs MI state. A measurement of this lifetime at $B = 355 \text{ G}$, corresponding to $a_{\text{CsCs}} \approx 2500 a_0$, is shown in Fig. 4(b) [17]. Below about $V_{\text{mix}}^{\text{Cs}} \approx 20 E_{\text{rec}}^{\text{Cs}}$, corresponding to $V_{\text{mix}}^{\text{Rb}} \approx 7.5 E_{\text{rec}}^{\text{Rb}}$, the lifetime is significantly reduced, in agreement with the loss of efficiency below the same value as found in the data shown in Fig. 4(a). We note that the Cs MI lifetime is much higher at lower values for B respectively a_{CsCs} at which we produce the Cs BEC.

We attribute the breakdown at higher values of V_{mix} to a breakdown of the Rb superfluid current [23, 24]. A given depth $V_{\text{mix}}^{\text{Rb}}$ thus defines a critical transport speed v_{crit} . Fig. 4(c) plots this critical speed as determined from data shown in Fig. 4(a) as a function of $V_{\text{mix}}^{\text{Rb}}$. Higher values of $V_{\text{mix}}^{\text{Rb}}$ determine a lower v_{crit} . Simple linear extrapolation of our data towards larger values of V_{mix} gives a zero critical speed at $V_{\text{mix}}^{\text{Rb}} \approx 11 E_{\text{rec}}^{\text{Rb}}$. Fig. 4(c) also plots the theory prediction of Ref. [23]. Evidently, our data is significantly below this prediction. Note that shifting the theory curve horizontally by $3.5 E_{\text{rec}}^{\text{Rb}}$ gives very good agreement. We have no explanation for the discrepancy between our data and the theory prediction. We note that for the data shown e.g. in Fig. 3(a) we have chosen a transport speed that is significantly below the critical speed, as indicated by the diamond in Fig. 4(c).

Evidently, our mixing procedure can be improved in various ways. Most obviously a higher lattice depth at the end of the mixing procedure will enhance the localization of Rb atoms to individual lattice sites and hence increase the pair formation probability. Increasing the speed for superfluid transport will reduce the time over which three-body loss processes take place. Finally, reducing the initial distance between the two atomic samples will reduce the distance over which superfluid transport for Rb has to be carried out. Ideally, one should place two pancake-shaped BECs directly parallel to each other and then merge the two samples along the tightly confined direction.

In conclusion, we have formed a low-entropy sample of bosonic RbCs Feshbach molecules in an optical lattice. The entropy per molecule can be estimated to $\approx 2k_{\text{B}}$ [17]. Note that this is an upper bound, as we, at this point, can only give a lower bound on the lattice filling

fraction. The molecules can now be transferred by STIRAP to the electronic and rovibrational ground state for the generation of a low-entropy dipolar quantum gas. In a previous publication, though starting from a different Feshbach level, we were able to demonstrate 90% STIRAP transfer efficiency [11]. This efficiency was limited by the comparatively large extent of the thermal sample with respect to the beam waists of the STIRAP laser beams. We expect that this efficiency can now be pushed towards 100% given the much more localized samples. When in the ground state and polarized by an external electric field, the dynamics of the gas will then be dominated by nearest-neighbor interactions with interaction strength on the order of $h \times 1$ kHz. This will allow us to study important problems in quantum many-body physics, such as the phase diagram of the Bose-Hubbard model extended by a long-range interaction term [25, 26].

We thank S. Mezinska for technical assistance and M. J. Mark and F. Meinert for fruitful discussions. We are grateful to C. R. Le Sueur for providing detailed data for the interspecies scattering length and on the molecular structure as shown in Fig. S2 of the Supplemental Material. We acknowledge support by the Austrian Science Fund (FWF) through the Spezialforschungsbereich (SFB) FoQuS within project P06 (FWF project number F4006-N23).

[1] C. Trefzger, C. Menotti, B. Capogrosso-Sansone, and M. Lewenstein, *J. Phys. B: At. Mol. Opt. Phys.* **44**, 193001 (2011).
[2] M. Baranov, M. Dalmonte, G. Pupillo, and P. Zoller, *Chem. Rev.* **112**, 5012 (2012).
[3] T. Lahaye, C. Menotti, L. Santos, M. Lewenstein, and T. Pfau, *Rep. Prog. Phys.* **72**, 126401 (2009).
[4] K. R. A. Hazzard, S. R. Manmana, M. Foss-Feig, and A. M. Rey, *Phys. Rev. Lett.* **110**, 075301 (2013).
[5] X. Deng, B. L. Altshuler, G. V. Shlyapnikov, and L. Santos, *Phys. Rev. Lett.* **117**, 020401 (2016).
[6] I. Bloch, J. Dalibard, and S. Nascimbène, *Nature Phys.* **8**, 267 (2012).
[7] K. Winkler, F. Lang, G. Thalhammer, P. van der Straten, R. Grimm, and J. Hecker Denschlag, *Phys. Rev. Lett.* **98**, 043201 (2007).
[8] J. G. Danzl, E. Haller, M. Gustavsson, M. J. Mark, R. Hart, N. Bouloufa, O. Dulieu, H. Ritsch, and H.-C. Nägerl, *Science* **321**, 1062 (2008).
[9] J. G. Danzl, M. J. Mark, E. Haller, M. Gustavsson, R. Hart, J. Aldegunde, J. M. Hutson, and H.-C. Nägerl, *Nat. Phys.* **6**, 265 (2010).
[10] K.-K. Ni, S. Ospelkaus, M. H. G. de Miranda, A. Pe'er, B. Neyenhuis, J. J. Zirbel, S. Kotochigova, P. S. Julienne, D. S. Jin, and J. Ye, *Science* **322**, 231 (2008).
[11] T. Takekoshi, L. Reichsöllner, A. Schindewolf, J. M. Hutson, C. R. Le Sueur, O. Dulieu, F. Ferlaino, R. Grimm, and H.-C. Nägerl, *Phys. Rev. Lett.* **113**, 205301 (2014).
[12] P. K. Molony, P. D. Gregory, Z. Ji, B. Lu, M. P. Köppinger, C. R. Le Sueur, C. L. Blackley, J. M. Hutson,

and S. L. Cornish, *Phys. Rev. Lett.* **113**, 255301 (2014).
[13] J. W. Park, S. A. Will, and M. W. Zwierlein, *Phys. Rev. Lett.* **114**, 205302 (2015).
[14] M. Guo, B. Zhu, B. Lu, X. Ye, F. Wang, R. Vexiau, N. Bouloufa-Maafa, G. Quéméner, O. Dulieu, and D. Wang, *Phys. Rev. Lett.* **116**, 205303 (2016).
[15] S. A. Moses, J. P. Covey, M. T. Miecnikowski, B. Yan, B. Gadway, J. Ye, and D. S. Jin, *Science* **350**, 659 (2015).
[16] J. P. Covey, S. A. Moses, M. Gärttner, A. Safavi-Naini, M. T. Miecnikowski, Z. Fu, J. Schachenmayer, P. S. Julienne, A. M. Rey, D. S. Jin, et al., *Nat. Comm.* **7**, 11279 (2016).
[17] See Supplemental Material for details on experiment timing, Feshbach states, convolution modelling, filling fraction and entropy, on-site interspecies interaction, Cs MI characterization, critical transport velocity, and magnetic field calibration, including Refs. [27–31].
[18] A. Lercher, T. Takekoshi, M. Debatin, B. Schuster, R. Rameshan, F. Ferlaino, R. Grimm, and H.-C. Nägerl, *Eur. Phys. J. D* **65**, 3 (2011).
[19] T. Weber, J. Herbig, M. Mark, H.-C. Nägerl, and R. Grimm, *Science* **299**, 232 (2003).
[20] T. Takekoshi, M. Debatin, R. Rameshan, F. Ferlaino, R. Grimm, H.-C. Nägerl, C. R. Le Sueur, J. M. Hutson, P. S. Julienne, S. Kotochigova, et al., *Phys. Rev. A* **85**, 032506 (2012).
[21] F. Meinert, M. J. Mark, E. Kirilov, K. Lauber, P. Weinmann, A. J. Daley, and H.-C. Nägerl, *Phys. Rev. Lett.* **111**, 053003 (2013).
[22] M. Berninger, A. Zenesini, B. Huang, W. Harm, H.-C. Nägerl, F. Ferlaino, R. Grimm, P. S. Julienne, and J. M. Hutson, *Phys. Rev. A* **87**, 032517 (2013).
[23] E. Altman, A. Polkovnikov, E. Demler, B. I. Halperin, and M. D. Lukin, *Phys. Rev. Lett.* **95**, 020402 (2005).
[24] J. Mun, P. Medley, G. K. Campbell, L. G. Marcassa, D. E. Pritchard, and W. Ketterle, *Phys. Rev. Lett.* **99**, 150604 (2007).
[25] B. Damski, L. Santos, E. Tiemann, M. Lewenstein, S. Kotochigova, P. Julienne, and P. Zoller, *Phys. Rev. Lett.* **90**, 110401 (2003).
[26] B. Capogrosso-Sansone, C. Trefzger, M. Lewenstein, P. Zoller, and G. Pupillo, *Phys. Rev. Lett.* **104**, 125301 (2010).
[27] C. R. Le Sueur, private communication.
[28] G. Thalhammer, K. Winkler, F. Lang, S. Schmid, R. Grimm, and J. Hecker Denschlag, *Phys. Rev. Lett.* **96**, 050402 (2006).
[29] D. Budker, D. F. Kimball, and D. P. DeMille, *Atomic Physics: An Exploration through Problems and Solutions* (Oxford University Press, Oxford, 2008), 2nd ed.
[30] D. Jaksch, C. Bruder, J. I. Cirac, C. W. Gardiner, and P. Zoller, *Phys. Rev. Lett.* **81**, 3108 (1998).
[31] D. A. Steck, *Cesium D line data*, available online at <http://steck.us/alkalidata>, revision 2.1.4 (2010).

SUPPLEMENTAL MATERIAL

Experimental timing

Details of a typical experimental sequence are given in Fig. S1. The sequence starts with the loading of the two BECs into the optical lattice and creating a Cs MI, followed by the transport of the Rb BEC, the Rb-Cs pair formation, the production and the subsequent detection of molecules. We denote the intensity in the dipole trapping beams by $I_{y,Rb}$, $I_{y,Cs}$, and I_x for the beams along the y -direction for the initial Rb and Cs dipole traps and for the beam joining the two samples along the transport x -direction, respectively (see Fig. 1(a) of the main article). In the course of the sequence, the lattice depth $V^{Cs} = 2.6V^{Rb}$, the Rb trap position x_{Rb} along the transport direction, the intensities $I_{y,Rb}$, $I_{y,Cs}$, and I_x , the magnetic offset field B , and the magnetic field gradient $|\nabla B|$ are ramped. Note that the Cs atoms see a 1.08 times larger trap frequency than the Rb atoms for a given dipole trap laser power.

Initially, the Rb BEC and the Cs BEC are spatially separated along the x -direction by $\approx 100 \mu\text{m}$ with $\nu_{Rb,x} = 38 \text{ Hz}$, $\nu_{Cs,x} = 10 \text{ Hz}$, $\nu_{Rb,y} = 14 \text{ Hz}$, $\nu_{Cs,y} = 15 \text{ Hz}$, $\nu_{Rb,z} = 39 \text{ Hz}$, and $\nu_{Cs,z} = 18 \text{ Hz}$. Here, $\nu_{Rb,x}$ denotes the trap frequency for the Rb trap in x -direction, and analogously for the other trap frequencies. The initial distance of the two BECs is large enough to avoid spilling from one sample into the other. In the course of the transport, while the confinement of the two samples is controlled by the intensities $I_{y,Rb}$, $I_{y,Cs}$, and I_x , it is strongly modified along the x -direction when the underlying dipole traps start to overlap. Beam steering to move the Rb trap along the x - and the z -directions is achieved by a two-axis translational piezo flexure stage onto which we have attached the fiber tip of the fiber that delivers the light for the Rb trap beam propagating in the y -direction. Beam steering is done with μm -precision as verified by in-situ absorption images. The initial gradient $|\nabla B| = 31.1 \text{ G/cm}$ levitates the Cs sample against gravity, but slightly overlevitates the Rb sample.

Upon loading both ensembles into the 3D optical lattice with a lattice spacing of $\lambda/2 = 532.25 \text{ nm}$ we drive the SF-to-MI phase transition for the Cs sample while leaving the Rb sample superfluid. For this, we exponentially increase the lattice depth to $V^{Cs} = V_{\text{mix}}^{Cs} = 20 E_{\text{rec}}^{Cs}$ ($V^{Rb} = 7.7 E_{\text{rec}}^{Rb}$). At the same time underlying Cs dipole trap is stiffened to assure that we create a clean one-atom MI shell for Cs.

Subsequently, the Rb sample is transported through the lattice towards and onto the Cs sample within typically 1500 ms by moving the underlying Rb dipole trap along the x -direction. The gradient $|\nabla B|$ is ramped to 30.1 G/cm in the course of the first 500 ms of the transport process for optimum levitation of Rb. We slightly

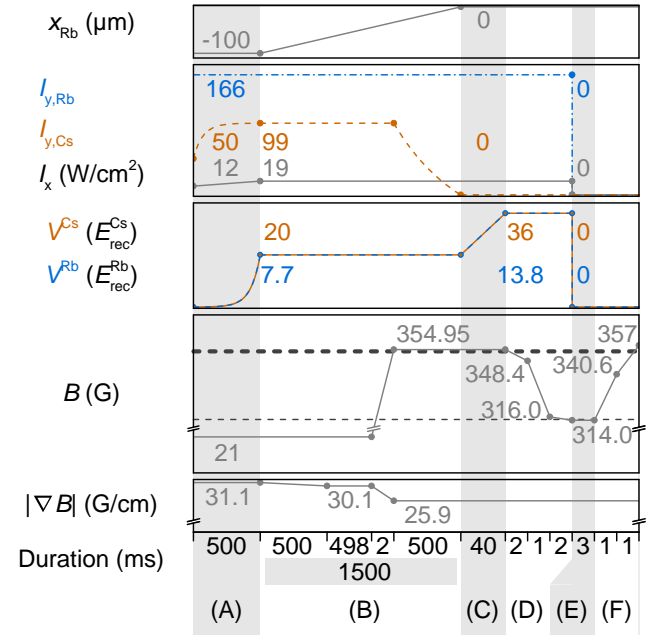


FIG. S1: (Color online). Typical timing sequence for the experimental cycle with typical values for the Rb trap position x_{Rb} along the transport direction, the beam intensities $I_{y,Rb}$, $I_{y,Cs}$, and I_x , the lattice depth $V^{Cs} = 2.6V^{Rb}$, the magnetic offset field B , and the magnetic field gradient $|\nabla B|$ as a function of time. The various experimental stages (A) lattice loading, (B) Rb transport, (C) Rb localization, (D) molecule formation, (E) Stern-Gerlach separation, and (F) dissociation and detection are indicated in the lower part of the diagram. The horizontal axis is not to scale.

adjust the vertical position of the Rb trap in the course of the transport for optimal overlap with the Cs sample.

After 998 ms of the transport, i.e. 502 ms before the Rb sample has reached its final position, the offset field B is ramped within 2 ms to the zero crossing for $a_{Rb,Cs}$ at 354.95 G. Simultaneously $|\nabla B|$ is adjusted to 25.9 G/cm to compensate for the change in the magnetic moment of Rb as B is changed. Within the last 500 ms of the transport the underlying Cs dipole trap beam along the y -direction is adiabatically turned off to avoid its influence on the final phase of the Rb transport.

As soon as the Rb transport is finished we increase the lattice depth V^{Cs} to $V_{\text{fin}}^{Cs} = 36 E_{\text{rec}}^{Cs}$ ($V_{\text{fin}}^{Rb} = 13.8 E_{\text{rec}}^{Rb}$) to drive the Rb sample into the MI regime and to form Rb-Cs atom pairs in the lattice. By adiabatically sweeping B within 2 ms over the pole of the Feshbach resonance at 355.74 G to 348.4 G we associate the paired atoms to weakly bound molecules (see the Zeeman diagram in Fig. S2). Subsequently, within 1 ms, we jump B to 316.0 G, where an avoided crossing is located that allows us to transfer the molecules into the second state by ramping B in 2 ms to 314.0 G (see Fig. S2 and the discussion in the next section). This final molecular state possesses a magnetic moment that significantly differs from

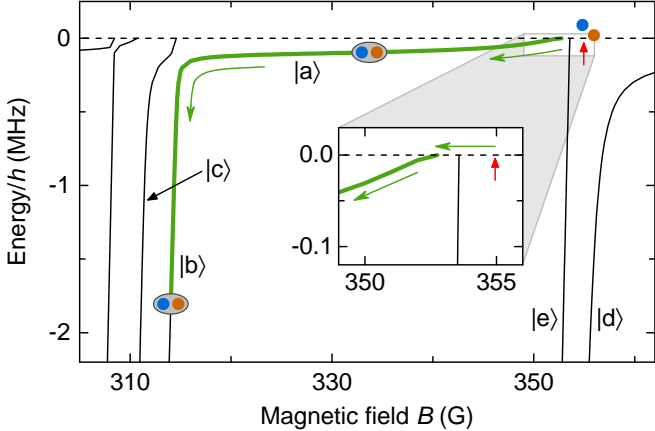


FIG. S2: (Color online). Zeeman diagram for the molecular states with $M_{\text{tot}} = 4$ just below the ground-state two-atom ($f_{\text{Rb}}, f_{\text{Cs}} = (1, 3)$) threshold. Energies as a function of B are given relative to the field-dependent dissociation threshold (horizontal dashed line). The red arrow marks the position of the Feshbach-resonance zero crossing at which Rb-Cs atom pairs are produced. The magneto-association path is indicated by the green arrows and the thick green line, first following state $|a\rangle$ and then ending in state $|b\rangle$ as B is lowered. The inset zooms into the resonance region, showing the zero-crossing position at 354.95 G (red arrow), an overlapping molecular state $|e\rangle$ hitting threshold at 353.57 G (black, nearly vertical line) and the pole of the Feshbach resonance at 352.74 G where state $|a\rangle$ hits threshold.

the one of the unbound atoms, allowing Stern-Gerlach separation of molecules and atoms. We switch off the dipole trap and lattice potentials abruptly and spatially separate the molecules from non-associated atoms within 3 ms time of flight. For detection we reverse the Feshbach association ramp to dissociate the molecules back to atoms. These atoms and also the atoms that were not subject to molecule formation are subsequently detected by standard absorption imaging.

Feshbach states

In the following we adopt the labelling $|n(f_{\text{Rb}}, f_{\text{Cs}})L(m_{f_{\text{Rb}}}, m_{f_{\text{Cs}}})M_{\text{tot}}\rangle$ of the Feshbach states used in Ref. [1], where a broader overview on the Rb-Cs Feshbach states and resonances is given. The number n indicates the vibrational level as counted from threshold (i.e. $n = -1$ refers to the least bound vibrational level, $n = -2$ is the second least bound vibrational level, etc.) and the quantum numbers f and m_f label the total atomic angular momentum and its projection onto

the B -field axis, respectively. The quantum number L (with s for $L = 0$, p for $L = 1$, d for $L = 2$ etc.) denotes the molecular rotational angular momentum and $M_{\text{tot}} = m_{f_{\text{Rb}}} + m_{f_{\text{Cs}}} + M_L$ is the sum of all projected angular momenta. Since here $M_{\text{tot}} = 4$ for all relevant states we omit M_{tot} .

For the mixing process and molecule creation we make use of a 2.21-G wide Rb-Cs Feshbach resonance, whose pole is located at 352.74 G. The background interspecies scattering length in the vicinity of this resonance is $a_{\text{RbCs}} = 654 a_0$ [2]. The Rb and Cs samples are initially overlapped at the zero crossing for a_{RbCs} at 354.95 G, indicated by the red arrow in Fig. S2. From there B is ramped to the pole of the resonance, jumping non-adiabatically a very narrow Feshbach resonance (with a width of 1.2 mG) located at 353.57 G caused by the molecular state $|e\rangle = |-6(2, 4)d(0, 2)\rangle$ [2] (see inset in Fig. S2). The atoms then enter a Feshbach state that initially is a combination of state $|a\rangle = |-1(2, 4)s(1, 3)\rangle$ and $|d\rangle = |-6(2, 4)s(0, 4)\rangle$ (green curve in the inset to Fig. S2). Upon further lowering B the state becomes $|a\rangle$. In order to allow the separation of molecules from unbound atoms via the Stern-Gerlach technique, an anti-crossing of molecular states at 315 G is used to adiabatically transfer the molecules from state $|a\rangle$ to $|b\rangle$. The latter one is together with state $|c\rangle$ a superposition of the molecular states $|-6(2, 4)d(0, 3)\rangle$ and $|-6(2, 4)s(1, 3)\rangle$. The exact composition of the molecular states is of importance for future work when the molecules are to be transferred by STIRAP from their weakly-bound state to their rovibronic ground state.

Convolution modelling

We characterize the overlap of the two atomic samples, as presented in Fig. 2 of the main article, by using a simple model that assumes two spheres of homogeneous density with radii r_1 and r_2 . The convolution $C(d)$ of two spheres as a function of the distance d between their centers is given by

$$C(d) = \frac{\pi}{12d} (r_1 + r_2 - d)^2 [d^2 + 2d(r_1 + r_2) - 3(r_1 - r_2)^2]$$

for partial overlap $|r_1 - r_2| < d < (r_1 + r_2)$. We allow for an asymmetric offset $N_{\text{RbCs}}^{\text{offset}}$ to account for the trailing tail that is observed in the experiment when convolving the samples along the transport x -direction. Setting $x_{\text{Cs}} = 0$ for the center of the Cs sample, the full fit function to the number of RbCs molecules N_{RbCs} then reads

$$N_{\text{RbCs}}(x_{\text{Rb}}) = \begin{cases} 0, & x_{\text{Rb}} \leq -(r_1 + r_2) \\ N_{\text{RbCs}}^{\max} \frac{C(-x_{\text{Rb}})}{C(|r_1 - r_2|)}, & -(r_1 + r_2) < x_{\text{Rb}} < -|r_1 - r_2| \\ N_{\text{RbCs}}^{\max}, & -|r_1 - r_2| \leq x_{\text{Rb}} \leq |r_1 - r_2| \\ (N_{\text{RbCs}}^{\max} - N_{\text{RbCs}}^{\text{offset}}) \frac{C(x_{\text{Rb}})}{C(|r_1 - r_2|)} + N_{\text{RbCs}}^{\text{offset}}, & |r_1 - r_2| < x_{\text{Rb}} < (r_1 + r_2) \\ N_{\text{RbCs}}^{\text{offset}}, & (r_1 + r_2) \leq x_{\text{Rb}} \end{cases}$$

For $r_1 \neq r_2$ the function has a characteristic volcano-like profile, where N_{RbCs}^{\max} defines the height the plateau when one sphere is fully enclosed by the other. The fit cannot attribute r_1 and r_2 to the individual species, however for a sufficiently large difference in the atom number we presume that the smaller radius belongs to the smaller sample (here Cs). Even though the atom samples possess some ellipticity due to the shape of their trapping potential and even though their densities are inhomogeneous, the fit should yield acceptable estimates for samples' radii along the direction of the convolution measurement. When compared to a simple calculation that assumes the formation of defect-free single-shell MIs the sample radii that result from the convolution-measurement fits are roughly 1 μm larger. This deviation is probably the result of a reduced density in the outer region of the MI as a result of non-zero temperatures. Note that the convolution measurement shows that we control the relative positioning of the two atom samples along the two steering axes to a much higher precision than the resolution of our imaging setup. It in particular allows us to calibrate a roughly 5- μm chromatic offset between the absorption images of the two species.

Filling fraction and entropy

We normalize the number of RbCs molecules N_{RbCs} by the number $N_{\text{Cs}}^{\text{BEC}}$ of atoms in the Cs BEC and thereby obtain a lower bound for the filling fraction of the RbCs molecules in the optical lattice when we assume a filling fraction of unity for the Cs MI right after lattice loading and full coverage of the Cs sample by a homogeneous density of Rb atoms. The first assumption is well fulfilled for the center region of the Cs MI (see section Cs MI characterization). The second assumption, however, is not necessarily fulfilled and can locally lead to an underestimation of the filling fraction. The Rb sample is elongated along the y -axis, therefore a significantly higher Rb atom number is required to fully cover the nearly spherical Cs MI. Although the initial Rb BEC is about twice as large as the Cs BEC, this requirement is not necessarily met, since 20%–50% of the Rb atoms are stuck in the lattice during transport. Furthermore, the Rb density is not homogeneous, especially since we are not yet able to drive the Rb sample deep into the MI regime. We note that

the elongation of the Rb sample is actually necessary to provide sufficient overlap since we have no handle on the relative position of the atom clouds along the y -axis and a small offset exists due to the fact that the focus of the Cs trapping beam is axial shifted from the intersection with the trapping beam that defines the transport axis.

Several aspects limit the filling fraction of the RbCs molecules: The finite lifetime of the Cs MI at high magnetic fields (see section Cs MI characterization) as well as losses during the overlapping process, which we attribute to interspecies three-body recombination, create vacancies in the Cs MI. Finite coverage of the Cs MI by the Rb sample and variations in the Rb density from $n_{\text{Rb}} = 1$ limit the overall pair formation efficiency. The loss of Cs atoms in absence of the Rb sample is about 15%. The number of Rb atoms that are lost during the mixing process (excluding atoms that are stuck on the way to the Cs sample during the transport) is about 1.6(1) times the number of additionally lost Cs atoms in presence of Rb. It therefore appears that this loss is dominated by the Rb-Rb-Cs three-body loss mechanism, further reducing the number of Cs atoms by 35% of the Cs BEC size. We observe an enhancement of the interspecies loss for slower transport velocities, which can be compensated by bringing the lattice depth V_{mix} closer to the critical value at which the superflow of Rb breaks down. This is not surprising considering that both the critical transport velocity and the three-body loss rate scale with the tunneling time in the optical lattice. In the end, about 60% of the remaining Cs atoms (30% of $N_{\text{Cs}}^{\text{BEC}}$) are paired with Rb and successfully form RbCs molecules.

For calculation of the molecules' entropy we assume that lattice sites occupied by unassociated atoms can be emptied, e.g. by a blow-away technique [3, 4], without affecting the molecular sample. The probability for an empty site is then $1 - p$, where p is the molecular filling fraction, and the entropy per molecule is [5]

$$s \approx \frac{k_{\text{B}}}{p} (p \ln(p) + (1 - p) \ln(1 - p)).$$

Taking $p = 30\%$ as a lower bound gives $s = 2k_{\text{B}}$. This value compares well with the one reported in Ref. [6].

On-site interspecies interaction

For moderate values of the interspecies scattering length a_{AB} the Hubbard on-site interaction between atoms A and B is given by

$$U_{AB} = \frac{4\pi\hbar^2}{2\mu_{AB}} a_{AB} \int w_A^*(\mathbf{r}) w_B^*(\mathbf{r}) w_B(\mathbf{r}) w_A(\mathbf{r}) d^3r.$$

Here, $\mu_{AB} = m_A m_B / (m_A + m_B)$ is the reduced mass and $w_{A,B}$ are the Wannier functions for A and B, respectively. Independent of the depth of the lattice we find that $U_{\text{RbCs}} = -U_{\text{RbRb}}$ for $a_{\text{RbCs}} = -82 a_0$.

Cs MI characterization

At low values for B (i.e. $B = 21$ G, where we form the Cs BEC) the Cs sample in the optical lattice is stable for many seconds irrespective of the lattice depth. Increasing B to high values (necessary to access the Rb-Cs Feshbach resonance and to tune the interspecies interaction) however changes the Cs intraspecies scattering length a_{CsCs} dramatically. For $B = 354.95$ G, where we perform the mixing procedure, a_{CsCs} reaches about $2500 a_0$ [7]. We emphasize that in this regime it is of crucial importance to drive the system deeply into the MI state to protect the Cs MI from enhanced Cs-Cs-Cs three-body loss.

We analyze the stability of the Cs MI at high values for B (see Fig. 4(b) of the main article) by preparing first a Cs MI at $B = 21$ G for a lattice depth V^{Cs} . We increase B within 2 ms to $B = 354.95$ G and then hold the sample for a variable hold time τ before lowering B again back to $B = 21$ G within another 2 ms. In the end the lattice is ramped down adiabatically and the BEC fraction of the Cs sample is determined. We find that the BEC fraction decays exponentially with τ and determine the $1/e$ -lifetime t_{MI} as a function of V^{Cs} . The result is plotted in Fig. 4(b) of the main article. We note that the decay of the Cs atom number due to Cs-Cs-Cs three-body losses is in general slower than the decay of the BEC fraction. To maintain a stable Cs MI state over the course of the 540 ms that the atoms spend at high values for B during the mixing process (see section Experimental timing) the mixing lattice depth $V_{\text{mix}}^{\text{Cs}}$ has to be at least $20 E_{\text{rec}}^{\text{Cs}}$ (diamond in Fig. 4(b)). Below that value a significant reduction in the RbCs molecule production efficiency is observed (see Fig. 4(a)).

We check that we produce a relatively clean single-atom MI shell by using a technique described in Ref. [8]. The lattice depth along the vertical axis is lowered to $10 E_{\text{rec}}^{\text{Cs}}$ to allow the atoms to tunnel and a potential tilt along this axis is applied adiabatically. When the tilt per lattice site approaches the Cs on-site interaction U_{CsCs} a quantum phase transition is driven to a density-wave ordered state where every other lattice site along

the tilt axis is occupied by a Cs-Cs atom pair. The Cs pairs are associated to weakly bound Cs_2 molecules by means of a magnetic Cs Feshbach resonance to determine the number of Cs pairs that were formed this way. We find that about 80% of the entire Cs sample forms pairs, comparable to the results presented in Ref. [8]. Such a high pair formation efficiency can only be achieved in a low-defect MI shell.

Critical transport velocity

The lattice depth V_{mix} that is used for mixing the two samples sets a critical transport velocity v_{crit} for transport of Rb [9]. Beyond v_{crit} the superflow becomes chaotic in regions with average filling $n_{\text{Rb}} = 1$, triggering superflow breakdown for the entire Rb sample. The Rb sample gets stuck close to its initial position and cannot follow the movement of the underlying Rb dipole trap.

In the vicinity of the SF-to-MI transition, for a 3D lattice, the critical quasimomentum that corresponds to the critical transport velocity v_{crit} is given by [9]

$$q_{\text{crit}} = \frac{\hbar k_{\text{rec}}}{\pi} \text{Re} \left[\sqrt{2(1 - u/u_c)} \right].$$

Here, $\hbar k_{\text{rec}} = h/\lambda$ is the recoil momentum set by the lattice light, and the interaction strength is $u = U_{\text{RbRb}}/J_{\text{Rb}}$, with the Hubbard interaction parameter U_{RbRb} and the tunneling matrix element J_{Rb} for Rb. The critical value for u , which marks the SF-to-MI quantum-phase transition [10], is $u_c \approx 34.8$, which is reached for $V_{\text{mix}}^{\text{Rb}} \approx 13.8 E_{\text{rec}}^{\text{Rb}}$. The group velocity with which the Rb sample moves through the lattice is defined by the dispersion relation of the lowest lattice band $E(q)$ as $v_g(q) = \partial E(q)/\partial q$ and allows us to calculate the critical transport velocity $v_{\text{crit}} = v_g(q_{\text{crit}})$ (dash-dotted line in Fig. 4(c) of the main article).

The value for the critical quasimomentum q_{crit} predicted in Ref. [9] was experimentally tested in Ref. [11] with a Rb sample in a sinusoidally moving 3D optical lattice and good agreement between theory and experiment was found. In our experiment we perform linear transport by means of the underlying dipole trap that moves at constant speed in the presence of a stationary 3D lattice. The breakdown in superfluid transport is reflected by an abrupt loss of pair formation efficiency as shown in Fig. 4(a) of the main article. Concomitantly, we find from in-situ absorption images that the Rb sample experiences sudden inhibition of transport. The critical transport velocity v_{crit} as determined from our data is much lower by at least a factor 2 than the one predicted by theory. Interestingly, our data is fit well by shifting the theoretical values by $3.5 E_{\text{rec}}^{\text{Rb}}$ towards shallower lattice depths (dashed line in Fig. 4(c)). The discrepancy between our experiment and theory merits further investigations.

Magnetic field calibration

The magnetic field B is calibrated by microwave spectroscopy. To assure that we work under the same conditions as in the molecule formation experiment we use the sequence for molecule creation in an optical lattice as described above (see also Fig. S1) but load only a Cs sample, create a Cs one-atom MI, and substitute the molecule creation procedure by a 20 ms microwave pulse. A microwave antenna, powered by a programmable microwave source with 5 W output, irradiates the Cs atoms and drives the π transition of the lowest Cs hyperfine states $|f_{\text{Cs}}, m_{f_{\text{Cs}}}\rangle = |3, 3\rangle$ to $|4, 3\rangle$. We measure the number of Cs atoms in state $|3, 3\rangle$ and $|4, 3\rangle$ by means of Stern-Gerlach separation as we scan the microwave frequency. We extract the resonance position from Gaussian fits to the data and calculate the corresponding value for B via the Breit-Rabi formula [12]. The values for B can then be converted to values for a_{RbCs} [2]. In this way we are able to determine the zero-crossing of the interspecies scattering length a_{RbCs} at 354.95 G with an accuracy of 17 mG. We note that the pole of the interspecies Feshbach resonance together with its adjacent zero crossing leave significant signatures in a different set of experiments in which we probe the interference contrast of the superfluid Rb sample as we scan across the Feshbach resonance. In particular, at a certain value for B we observe a drastic loss of interference contrast. This we associate with the pole of the resonance. The position of the pole agrees with what we expect from our B -field calibration.

Magnetic field stability is crucial during the mixing process when $B \approx 355$ G. The most dominant magnetic noise contributions are at multiples of the line frequency 50 Hz. A feed-forward technique allows us to suppress Fourier components at 50 Hz, 100 Hz, 150 Hz, and 250 Hz. For this, a pick-up coil senses their phase and amplitude. During the mixing procedure these Fourier components are then added to B with a π phase shift synchronized to line. We thereby suppress the total mag-

netic field noise down to 50 mG rms, corresponding to about $15-a_0$ rms uncertainty for the interspecies scattering length in the vicinity of its zero crossing. The magnetic field gradient $|\nabla B| = 25.9$ G/cm causes an additional shift of $16 a_0$ across the typical 18- μm atom-sample diameter.

- [1] T. Takekoshi, M. Debatin, R. Rameshan, F. Ferlaino, R. Grimm, H.-C. Nägerl, C. R. Le Sueur, J. M. Hutson, P. S. Julienne, S. Kotochigova, et al., *Phys. Rev. A* **85**, 032506 (2012).
- [2] C. R. Le Sueur, private communication.
- [3] G. Thalhammer, K. Winkler, F. Lang, S. Schmid, R. Grimm, and J. Hecker Denschlag, *Phys. Rev. Lett.* **96**, 050402 (2006).
- [4] J. G. Danzl, M. J. Mark, E. Haller, M. Gustavsson, R. Hart, J. Aldegunde, J. M. Hutson, and H.-C. Nägerl, *Nat. Phys.* **6**, 265 (2010).
- [5] D. Budker, D. F. Kimball, and D. P. DeMille, *Atomic Physics: An Exploration through Problems and Solutions* (Oxford University Press, Oxford, 2008), 2nd ed.
- [6] S. A. Moses, J. P. Covey, M. T. Miecnikowski, B. Yan, B. Gadway, J. Ye, and D. S. Jin, *Science* **350**, 659 (2015).
- [7] M. Berninger, A. Zenesini, B. Huang, W. Harm, H.-C. Nägerl, F. Ferlaino, R. Grimm, P. S. Julienne, and J. M. Hutson, *Phys. Rev. A* **87**, 032517 (2013).
- [8] F. Meinert, M. J. Mark, E. Kirilov, K. Lauber, P. Weinmann, A. J. Daley, and H.-C. Nägerl, *Phys. Rev. Lett.* **111**, 053003 (2013).
- [9] E. Altman, A. Polkovnikov, E. Demler, B. I. Halperin, and M. D. Lukin, *Phys. Rev. Lett.* **95**, 020402 (2005).
- [10] D. Jaksch, C. Bruder, J. I. Cirac, C. W. Gardiner, and P. Zoller, *Phys. Rev. Lett.* **81**, 3108 (1998).
- [11] J. Mun, P. Medley, G. K. Campbell, L. G. Marcassa, D. E. Pritchard, and W. Ketterle, *Phys. Rev. Lett.* **99**, 150604 (2007).
- [12] D. A. Steck, *Cesium D line data*, available online at <http://steck.us/alkalidata>, revision 2.1.4 (2010).